HHS Public Access

Author manuscript

Cryobiology. Author manuscript; available in PMC 2017 October 01.

Published in final edited form as:

Cryobiology. 2016 October ; 73(2): 196–202. doi:10.1016/j.cryobiol.2016.07.012.

Thermal conductivity of the cryoprotective cocktail DP6 in cryogenic temperatures, in the presence and absence of synthetic ice modulators

Lili E. Ehrlich, **Jonathan A. Malen**, and **Yoed Rabin**[1]

Department of Mechanical Engineering, Carnegie Mellon University, Pittsburgh, Pennsylvania, 15213

Abstract

The thermal conductivity of the cryoprotective agent (CPA) cocktail DP6 in combination with synthetic ice modulators (SIMs) is measured in this study, using a transient hot-wire method. DP6 is a mixture of 3M dimethyl sulfoxide (DMSO) and 3M propylene glycol, which received significant attention in the cryobiology community in recent years. Tested SIMs include 6% 1,3Cyclohexanediol, 6% 2,3Butanediol, and 12% PEG400 (percentage by volume). This study integrates the scanning cryomacroscope for visual verification of crystallization and vitrification events. It is demonstrated that the thermal conductivity of the vitrifying CPA cocktail decreases monotonically with the decreasing temperature down to −180°C. By contrast, the thermal conductivity of the crystalline material increases with decreasing temperature in the same temperature range. Results of this study demonstrate that the thermal conductivity may vary by three fold between the amorphous and crystalline phases of DP6 below the glass transition temperature of DP6 (T_g = −119°C). The selected SIMs demonstrate the ability to inhibit crystallization in DP6, even at subcritical cooling rates. An additional ice suppression capability is observed by the Euro-Collins as a vehicle solution, disproportionate to its volume ratio in the cocktail. The implication of the observed thermal conductivity differences between the amorphous and crystalline phases of the same cocktail on cryopreservation simulations is significant in some cases and must be taken into account in thermal analyses of cryopreservation protocols.

Keywords

Thermal Conductivity; Vitrification; Crystallization; Cryogenic Temperatures; Measurements; DP6; Synthetic Ice Modulators

Introduction

Cryopreservation success revolves around the control of the kinetics of ice crystallization—the cornerstone of cryoinjury. Controlling the formation of ice is achieved by introducing cryoprotective agents (CPAs) into the specimen and controlling its thermal history. *Classical cryopreservation*—the preservation of a specimen using low CPA concentration—

[1]Corresponding author: rabin@cmu.edu.

essentially aims at limiting ice formation to the extracellular space and has shown successful results with small samples [14], typically in the range of μm to mm. Unfortunately, the extracellular ice formation inherent to classical cryopreservation techniques cannot be tolerated by organized, complex, multicellular systems, which necessitates alternative means for scaling up cryopreservation to bulky tissues and organs [23,25].

Vitrification is an alternative approach to classical cryopreservation, where the specimen is permeated with a high-concentration CPA cocktail and cooled rapidly in an effort to completely avoid ice crystallization (*vitreous* means *glassy* in Latin). While vitrification in biological systems was initially investigated by Luyet in 1937, it remained largely unexplored until the 1980's [10,25]. Vitrification is based on the temperature dependency of the CPA viscosity, which increases exponentially with decreasing temperature [16]. If the material is cooled fast enough, such that the typical time scale for crystallization is longer than the typical time scale for cooling, the viscosity gets to such extremely high values that the material is trapped in an amorphous state and behaves as solid for all practical purposes. The temperature threshold below which the vitrified material is considered solid is commonly known as the glass transition temperature, T_g.

Successful large-size vitrification brings about three competing needs: (i) to increase the CPA concentration in order to compensate for the decreasing cooling rate at the center of a large specimen (the cooling rate threshold to ensure vitrification decreases with the increasing concentration); (ii) to decrease the CPA concentration in order to minimize its toxicity effects [8,9]; and, (iii) to decrease the cooling rate within the glassy state in order to reduce thermo-mechanical stress, which may lead to structural damage [22]. Note that the cooling rate is only one among several factors that may elevate thermo-mechanical stresses to hazardous levels [22]. The above competing needs outline an optimization problem, combining concepts from cryobiology, thermal design, and solid mechanics [25].

In an effort to level the playing field for the complex optimization process of the large-size vitrification problem, additional compounds, known as synthetic ice modulators (SIMs), may be combined with the CPA cocktail [7]. In broad terms, SIMs are added not to prevent ice nucleation but to inhibit ice growth, where successful cryopreservation in the presence of limited amounts of small crystals has already been demonstrated to be feasible in the case of blood vessels [1]. The current line of research aims at investigating physical properties relevant to vitrification in the presence of SIMs.

Optimizing the cryopreservation problem requires predictive tools, such as bioheat transfer simulations, to evaluate the likelihood of vitrification, ice nucleation, and crystal growth. Computer simulations of vitrification require knowledge on the thermophysical properties of the material, which represents a relatively uncharted area of research [5,6]. The current study focuses on the thermophysical property of thermal conductivity, which is a quantity indicating how well the material can transfer heat at steady-state. When the thermal conductivity is divided by the volumetric specific heat (a measure of the amount of energy required to elevate the temperature of a unit volume of the material by one degree), the quotient indicates how fast thermal information can travel through the domain—this quantity

is known as thermal diffusivity. The thermal diffusivity is a subject matter of concurrent studies by the current research team.

Materials and Methods

Experimental Setup

The experimental setup used in this study has been presented previously [6] and is described here in brief only, for the completeness of presentation. The experimental setup consists of: (i) the scanning cryomacroscope [11], which enables visualization of vitrification, and (ii) a transient hot-wire set-up for simultaneously measuring thermal conductivity [12,15]. With reference to Fig. 1, a hot-wire sensor is immersed in the CPA cocktail, contained in a cuvette, and placed on the experimental stage of the cryomacroscope. During experiments, the cryomacroscope is loaded on top of a controlled-rate cooling chamber (Kryo 10–16 chamber with a Kryo 10–20 controller, Planer Ltd., UK).

With reference to Fig. 1, a 75 mm platinum wire is mounted onto a three-dimensional (3D) printed ABS cuvette cap. The hot-wire sensor is immersed in the specimen, acting concurrently as a heater and as a resistance temperature sensor. Step-like Joule heating is imposed on the wire for a pre-specified duration by a constant current source (Model 6221, Keithley Instruments, Inc., Ohio), while a digital multimeter (Model 34401A, Keysight Technologies, Inc., Santa Rosa, CA) measures the transient resistance change ΔR of the wire. The temperature rise due to heating, ΔT, is extracted from the relationship between temperature and resistance of the wire (platinum):

$$\Delta T = \frac{\Delta R}{\beta R_{ref}} \quad (1)$$

where ΔR is the change in resistance during heating, β is the coefficient of electrical resistance, and R_{ref} is a reference resistance corresponding to the specific wire.

The transient thermal response of the wire to heating is fitted against an analytical solution of a radial heat diffusion problem, and the thermal conductivity is extracted from the data using:

$$k_{sample} = \frac{q/4\pi}{d(\Delta T)/d(\ln t)} \quad (2)$$

where t is the time since the onset of heating and q is the heat generation rate in the platinum wire per unit length. All details including modeling assumptions are described in [6]. The duration of each thermal conductivity measurement is 0.5 s, which is triggered every 40 s during the rewarming phase of the cryogenic protocol. With a transient wire response obtained at a frequency of 60 Hz, each extracted thermal conductivity value represents curve fitting over 30 data points. The rewarming phase was selected as a choice of practice, where

the quality of temperature control is higher and the resulting uncertainty in measurements is smaller [6].

In order to use Eq. (2) during constant-rate rewarming of the bulk sample, the temperature variation of the bulk sample is subtracted from that measured during heating with the transient hot-wire [6]. Uncertainty in thermal conductivity measurements using the above setup and analysis method is estimated to be up to 0.03W/m-K [6]. Based on the results presented below, this uncertainty ranges from 3% to 10% of the measured value for the extreme cases of crystallized and vitrified cocktails at −180°C, respectively (i.e., the highest and lowest thermal conductivity measurements, respectively).

Thermal Protocol

Consistent with previous studies [1,6,11,19,21], the thermal protocol comprises six phases: (i) precooling to approximately 12°C, to reduce condensation on the cryomacroscope optics; (ii) rapid cooling at a rate H_1 to temperature T_1 (typically 20°C above T_g); (iii) slow cooling at a rate H_2 down to storage temperature T_s; (iv) hold time t_s until the specimen reaches thermal equilibrium at the storage temperature; (v) passive rewarming at a rate H_3 up to −100°C; and, (vi) controlled-rate rewarming at a rate of H_4 back to room temperature. The passive cooling below −100°C was selected to eliminate temperature oscillations inherent to the controlled-rate cooling chamber in very low temperatures (see hardware specification above). Furthermore, since significant crystallization is only expected to occur well above that temperature threshold, the uncontrolled cooling is not expected to affect thermal conductivity measurements. Figure 2 displays representative thermal histories as measured from a temperature sensor (T-type thermocouple) attached to the inner surface of the cuvette. Table 1 lists the specific thermal history values used in the current study for the various compounds measured.

In particular three representative initial cooling rates were selected (H_1) to investigate the thermal conductivity within the temperature range most prone to crystallization (investigated rates of 1°C/min to 50°C/min). At lower temperatures, slow cooling and rewarming rates (H_2 and H_3, respectively) were selected to prevent fracturing and possibly damaging the hot-wire (−2°C/min for cooling and an average of 1.7°C/min during passive rewarming). In some experiments the sample was cooled to the lower limit of the cooling chamber, −180°C, while in other experiments a temperature of −130°C was selected, which decreased the likelihood of fracturing in the glassy state [11]. Note that T_g for DP6 is −119°C [19].

Materials Tested

This study is focused on DP6 in the absence and presence of SIMs. DP6 is a mixture of 3M DMSO and 3M propylene glycol. Consistent with previous studies [7], this study uses Euro-Collins (EC) as a vehicle solution for DP6 but selected experiments were also conducted in the absence of Euro-Collins for reference (i.e, DP6 in pure water). Consistent with a recent study [7], DP6 experiments were conducted with one of the following SIMs: 6% 1,3 Cyclohexanediol (1,3CHD); 6% 2,3 Butanediol (2,3BD), and 12% PEG400 (percentage by volume). All solutions were frozen and thawed three times prior to experimentation to remove dissolved gases, which might affect the readings.

Results and Discussion

Figure 3 displays experimental results for DP6, DP6+SIMs, and previously published data for 6M DMSO for reference. Due to the close range of thermal conductivity data for all the SIM-based cocktails tested, the corresponding results are displayed as a range only in Fig. 3, while the specific distribution for the cocktails is presented in Fig. 4. Table 2 lists least-square, best-fit polynomial coefficients for the data displayed in Figs. 3 and 4, as a service for future analyses of thermal effects during SIM-based cryopreservation by vitrification (coefficient values were determined by the Matlab function polyfit, while the polynomial order was defined by the authors).

Note in Fig. 3 a data gap around −100°C to −80°C, which is associated with transitioning from passive to active rewarming during experimentation [6]. Due to overshooting of the temperature control system of the cooling chamber, the certainty in thermal conductivity measurements within this range is unknown and the corresponding data are omitted. In several experiments at the higher cooling rates (H_1 = 50°C/min) the hot-wire sensor was damaged above −100°C due to residual stress formed during cooling. Hence, data are missing from those experiments in Figs. 3 and 4, and Table 2 at higher temperatures.

Based on cryomacroscopy video analysis, vitrification occurred in all experiments where a SIM was added to the DP6, regardless of the SIM type; the vitrified material appears transparent while the crystalline material appears opaque [6]. This observation is consistent with the relatively low thermal conductivity characteristic of amorphous materials that is shown in Fig. 3. By contrast, in the absence of SIMs, DP6 in pure water crystallized at cooling rates below the critical value for vitrification, which is 40°C/min for DP6 [19]. This observation is consistent with the relatively high thermal conductivity displayed in Fig. 3, which is characteristic of crystalline solids.

It can further be seen from Fig. 3 that, in general, the thermal conductivity of the vitrified material decreases with the decreasing temperature, while the thermal conductivity of the crystalline material increases with the decreasing temperature. At much lower temperatures, the trend for crystalline materials is expected to reverse due to the decreasing population of energy carriers (i.e., phonons), but this is out of the range for current cryobiology applications. Disordered materials, such as a vitrified CPA, tend to have thermal conductivity values that are orders of magnitude lower than their crystalline counterparts, with dramatic effects on heat transfer analyses [17]. This difference is associated with the long-range order present in crystalline materials, which enables efficient thermal transport by phonons that arise from cooperative vibration of the molecules in the lattice. By comparison, disordered materials are poor transmitters of thermal energy due to the resulting uncorrelated vibrations [3,4].

Rewarming Phase Crystallization (RPC)

Cryomacroscope video recording and analysis of experimental data can help in identifying crystallization events, but cannot be used to quantify the extent of crystallization. For example, when DP6 is cooled at 50°C/min, it shows a lower thermal conductivity than when it is cooled at 5°C/min (Fig. 3), which suggests a reduced portion of crystals, or reduced

grain sizes, in the domain with the increased cooling rate. However, Fig. 3 also shows up to 10% higher thermal conductivity for DP6 cooled at 5°C/min than 2.5°C/min, which is counter-intuitive and represents the exception when compared with other solutions tested. The reason for this inverted difference is unknown but it can be the result of more favorable conditions to crystallization unrelated to the thermal history, such as dissolved gases or other nucleators. Either way, this is an indirect indication of the statistical nature of the onset and progression of crystallization in those non-equilibrium conditions. Note that the critical cooling rate reported in the literature is based on differential scanning calorimetric (DSC) studies, which use microliter-size samples, while the current data is generated for milliliter-size samples, and it is possible that the tendency to crystallize also increases with the sample size [2,13,26].

In particular for DP6 in the absence of SIMs subject to a cooling rate of 50°C/min, it can be seen from Fig. 3 that the thermal conductivity gradually increases with temperature between −100°C and about −70°C, but then exhibits a rapid increase up to about −55°C, followed by decreasing thermal conductivity representative of a crystalline material. This effect is associated with the phenomenon of RPC, which is an inclusive term combining crystal growth from nuclei already developed during cooling (also known as recrystallization) and crystal formation during rewarming (also known as devitrification). In general, RPC occurs when the viscosity of the material decreases with increasing temperature, while the material is still unstable below its heterogeneous nucleation temperature (about −35°C for DMSO at a similar concentration for reference [20]; not fully characterized for DP6) [19]. Given the much lower thermal conductivity values of DP6 when mixed with SIMs and cooled at 50°C/min, it is concluded that DP6 in the absence of SIMs already contains a significant portion of crystals from the cooling phase of the cryogenic protocol, and the related observed effect during rewarming is recrystallization.

Vehicle solution effects on DP6 vitrification in the absence of SIMs

It can be seen from Fig. 3 that DP6+EC behaves differently than DP6 in pure water for the same cooling rates in terms of the effect of RPC on thermal conductivity. For example, DP6+EC cooled at 2.5°C/min displays thermal conductivity of a vitrified material at the early stage of rewarming, up to about −65°C, and then it displays the effect of RPC.

The EC solution is designed to maintain ionic and hydraulic balance in cells at cold temperatures [24]. In particular, EC incorporates 0.194 M glucose which is a known glass promoting agent but in a very low concentration compared with the overall 6M concentration of DP6. This observation is of significance in the design of cryopreservation solutions, as the effects of vehicle solutions on the likelihood of vitrification may be overlooked.

Figure 5 displays the combined effects of cooling rate and the presence of EC on thermal conductivity at a temperature of −121°C (2°C below the glass transition temperature for DP6). For DP6 in the absence of EC and SIMs, the thermal conductivity decreases by 56% when the cooling rate is increased from 5°C/min to 50°C/min. For the case of DP6 with EC, thermal conductivity only decreases by 6% between the same cooling rates. Also note that the absolute value of thermal conductivity of DP6+EC is almost the same as that of

DP6+SIMs, Fig. 3. Clearly, EC plays a significant role in glass promotion and its effect on thermal conductivity.

The effects of SIMs on DP6 vitrification

The monotonic decrease in thermal conductivity with the decreasing temperature, highlighted as a gray band in Fig. 3, is a hallmark of amorphous materials (e.g., PMMA, glycerol). Although all DP6 solutions with SIM components have vitrified, resulting in a narrow range of thermal conductivity values over the temperature range studied, the thermal history for each cocktail can provide further insight on the process, as displayed in Fig. 4.

Note that solute precipitation from DP6+SIMs in EC has been reported recently [18], which affected opacity of the vitrified material, but did not affect the likelihood of crystallization or fracturing. The current study suggests that the thermal conductivity is not affected by solute precipitation at cryogenic temperatures as well. However, a very moderate effect of EC on thermal conductivity has been observed above the heterogeneous nucleation temperature (above about −35°C), which may be related to molecular mobility when the viscosity of the material is relatively low. At 0°C for example, an average lower thermal conductivity of 11% and 7% was measured for DP6+PEG400+EC and DP6+13CHD+EC, when compared with the same cocktails in the absence of EC.

For DP6+23BD, Fig. 4, a noticeable effect in thermal conductivity can be observed in the temperature range between −62°C and −31°C, with a maximum value at −45°C. This increase in thermal conductivity is likely to be the result of RPC and the apparent increase in thermal conductivity value may be a computational artifact using Eq. (2) within the same temperature range, rather than being an intrinsic property of the material. Note that once crystallization initiates, the thermal history in the specimen may be altered by the energy required for crystal nucleation and growth, which increases the uncertainty in applying the solution presented by Eq. (2). For example, heat is absorbed by the phase change process at a constant temperature and as a result the hot-wire interpretation is enhanced thermal conductivity. Even a very mild RPC would be picked up by the sensitive experimental system for thermal conductivity measurements used in this study. As pointed out above, the extent of vitrification can be measured with DSC, which is the subject matter of a parallel study. For DP6+23BD+EC, such RPC artifacts are not observed. This suggests that EC has played a part in suppression of RPC.

It can be concluded from the results presented in Fig. 4 that DP6+PEG400 is the best glass promoting cocktail and DP6+23BD is the worst out of the selection tested, except when used with EC. While RPC could have been avoided by increasing the rewarming rates, the corresponding values are above the range of the testing capabilities of the current system. For future thermal analyses, given the functional behavior of thermal conductivity with temperature, one can linearly interpolate the thermal conductivity within the RPC range by using its boundary values.

A very moderate effect of the cooling rate of DP6+SIM on its thermal conductivity can be observed from Fig. 5, within the tested range, measured in only a few percent. This difference suggests that each cocktail is mostly vitrified, which may greatly simplify future

computational cryobiology studies. It is also a reminder that the SIMs are not necessarily added to prevent ice nucleation but to further suppress ice growth.

Summary and Conclusions

The thermal conductivity of DP6 in combination with SIMs and EC has been measured using a hot-wire transient method. This experimental study used a scanning cryomacroscope for visual verification of crystallization and vitrification events. It is demonstrated that the thermal conductivity of the vitrifying CPA cocktail decreases monotonically with the decreasing temperature down to −180°C. By contrast, the thermal conductivity of the crystalline material increases with the decreasing temperature in the same temperature range.

Results of this study demonstrate that the thermal conductivity may vary by three fold between the amorphous and crystalline phases of DP6 below the glass transition temperature. However, the current experimental setup does not permit the quantification of the extent of crystallization in terms of volume ratio. Results of this study further demonstrate the ability of SIMs to decrease the extent of crystallization in DP6, even at subcritical cooling and rewarming rates. Finally, results of this study demonstrate an additional ice suppression capability of EC, which may be disproportionate to its volume ratio in the cocktail.

The implications of the observed thermal conductivity differences between the amorphous and crystalline phases of the same CPA cocktail on cryopreservation simulations is significant. In broad terms, the lower thermal conductivity in the amorphous state creates less favorable conditions to maintain the high cooling and rewarming rates at the center of large specimens that are required to ensure vitrification. In turn, when partial crystallization occurs within the specimen, the structural integrity of the material may be compromised due to differential thermal expansion between the crystallized and the amorphous regions. Hence, thermal conductivity data is not only critical for the prediction of the likelihood of vitrification, but also for the prediction of structural damage in cryopreservation protocols.

When SIMs are successfully applied, the thermal conductivity of the CPA+SIM cocktail is essentially the same as that of the vitrified CPA. The benefit for large-size cryopreservation is that the addition of SIMs lowers the critical cooling rates required for successful vitrification. Unfortunately, given the kinetics of ice crystallization and also the path-dependent nature of the cryopreservation process, it is difficult to predict a priori when significant crystallization will occur for a particular combination of CPA, SIMs, vehicle solution, and specific thermal history. Hence, characterization of thermal conductivity is most applicable if performed by mimicking the specific thermal history expected within a large specimen with the specific set compounds.

Acknowledgments

This work has been funded in part by the Dowd Fellowship from the College of Engineering at Carnegie Mellon University. The authors would like to thank Philip and Marsha Dowd for their financial support and encouragement. This work has also been funded in part by the National Heart Lung and Blood Institute (NHLBI, R01HL127618)

References

1. Baicu S, Taylor MJ, Chen Z, Rabin Y. Cryopreservation of carotid artery segments via vitrification subject to marginal thermal conditions: Correlation of freezing visualization with functional recovery. Cryobiology. 2008; 57:1–8. [PubMed: 18490009]
2. Baudot A, Alger L, Boutron P. Glass-forming tendency in the system water-dimethyl sulfoxide. Cryobiology. 2000; 40:151–158. [PubMed: 10788314]
3. Cahill DG, Pohl RO. Lattice Vibrations and Heat Transport in Crystals and Glasses. Annu Rev Phys Chem. 1988; 39:93–121.
4. Cahill DG, Pohl RO. Heat flow and lattice vibrations in glasses. Solid State Commun. 1989; 70:927–930.
5. Choi J, Bischof JC. Review of biomaterial thermal property measurements in the cryogenic regime and their use for prediction of equilibrium and non-equilibrium freezing applications in cryobiology. Cryobiology. 2010; 60:52–70. [PubMed: 19948163]
6. Ehrlich LE, Feig JSG, Schiffres SN, Malen JA, Rabin Y. Large Thermal Conductivity Differences between the Crystalline and Vitrified States of DMSO with Applications to Cryopreservation. PLoS ONE. 2015; 10:e0125862. [PubMed: 25985058]
7. Eisenberg DP, Taylor MJ, Rabin Y. Thermal expansion of the cryoprotectant cocktail DP6 combined with synthetic ice modulators in presence and absence of biological tissues. Cryobiology. 2012; 65:117–125. [PubMed: 22579521]
8. Fahy GM. The relevance of cryoprotectant “toxicity” to cryobiology. Cryobiology. 1986; 23:1–13. [PubMed: 3956226]
9. Fahy GM, Levy DI, Ali SE. Some emerging principles underlying the physical properties, biological actions, and utility of vitrification solutions. Cryobiology. 1987; 24:196–213. [PubMed: 3595164]
10. Fahy GM, MacFarlane DR, Angell CA, Meryman HT. Vitrification as an approach to cryopreservation. Cryobiology. 1984; 21:407–426. [PubMed: 6467964]
11. Feig JSG, Rabin Y. The scanning cryomacroscope – A device prototype for the study of cryopreservation. Cryogenics. 2014; 62:118–128. [PubMed: 25484372]
12. Healy JJ, de Groot JJ, Kestin J. The theory of the transient hot-wire method for measuring thermal conductivity. Phys BC. 1976; 82:392–408.
13. Hey JM, MacFarlane DR. Crystallization of Ice in Aqueous Solutions of Glycerol and Dimethyl Sulfoxide. 1. A Comparison of Mechanisms. Cryobiology. 1996; 33:205–216. [PubMed: 8812100]
14. Mazur, P. Life Frozen State. CRC Press; New York: 2004. Principles of Cryobiology; p. 3-65.
15. Nagasaka Y, Nagashima A. Absolute measurement of the thermal conductivity of electrically conducting liquids by the transient hot-wire method. J Phys [E]. 1981; 14:1435.
16. Noday DA, Steif PS, Rabin Y. Viscosity of cryoprotective agents near glass transition: a new device, technique, and data on DMSO, DP6, and VS55. Exp Mech. 2009; 49:663–672. [PubMed: 23226839]
17. Rabin Y. The effect of temperature-dependent thermal conductivity in heat transfer simulations of frozen biomaterials. Cryo Letters. 2000; 21:163–170. [PubMed: 12148047]
18. Rabin Y, Taylor MJ, Feig JSG, Baicu S, Chen Z. A new cryomacroscope device (Type III) for visualization of physical events in cryopreservation with applications to vitrification and synthetic ice modulators. Cryobiology. 2013; 67:264–273. [PubMed: 23993920]
19. Rabin Y, Taylor MJ, Walsh JR, Baicu S, Steif PS. Cryomacroscopy of vitrification, Part I: A prototype and experimental observations on the cocktails VS55 and DP6. Cell Preserv Technol. 2005; 3:169–183. [PubMed: 16721425]
20. Rasmussen DH, Mackenzie AP. Phase Diagram for the System Water–Dimethylsulphoxide. Nature. 1968; 220:1315–1317. [PubMed: 5701346]
21. Steif PS, Palastro M, Wan C, Baicu S, Taylor MJ, Rabin Y. Cryomacroscopy of vitrification, Part II: Experimental observations and analysis of fracture formation in vitrified VS55 and DP6. Cell Preserv Technol. 2005; 3:184–200. [PubMed: 16900261]

22. Steif PS, Palastro MC, Rabin Y. The Effect of Temperature Gradients on Stress Development during Cryopreservation via Vitrification. Cell Preserv Technol. 2007; 5:104–115. [PubMed: 18185851]

23. Taylor MJ, Baicu S. Review of vitreous islet cryopreservation. Organogenesis. 2009; 5:155–166. [PubMed: 20046679]

24. Taylor MJ, Campbell LH, Rutledge RN, Brockbank KGM. Comparison of Unisol with Euro-Collins solution as a vehicle solution for cryoprotectants. Transplant Proc. 2001; 33:677–679. [PubMed: 11267013]

25. Taylor, MJ., Song, YC., Brockbank, KGM. Life Frozen State. CRC Press; New York: 2004. Vitrification in Tissue Preservation: New Developments; p. 603-641.

26. Yinnon H, Uhlmann DR. A kinetic treatment of glass formation V: Surface and bulk heterogeneous nucleation. J Non-Cryst Solids. 1981; 44:37–55.

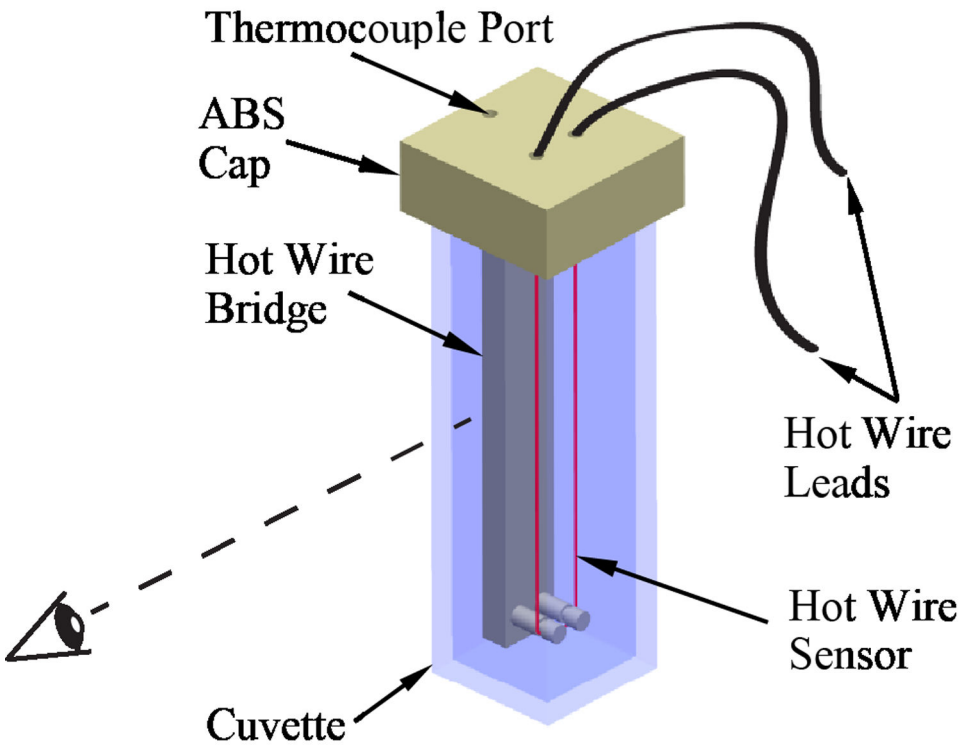

Figure 1.
Schematic illustration of the transient hot-wire sensor setup; the dashed line represents the direction of visualization by the scanning cryomacroscope [6].

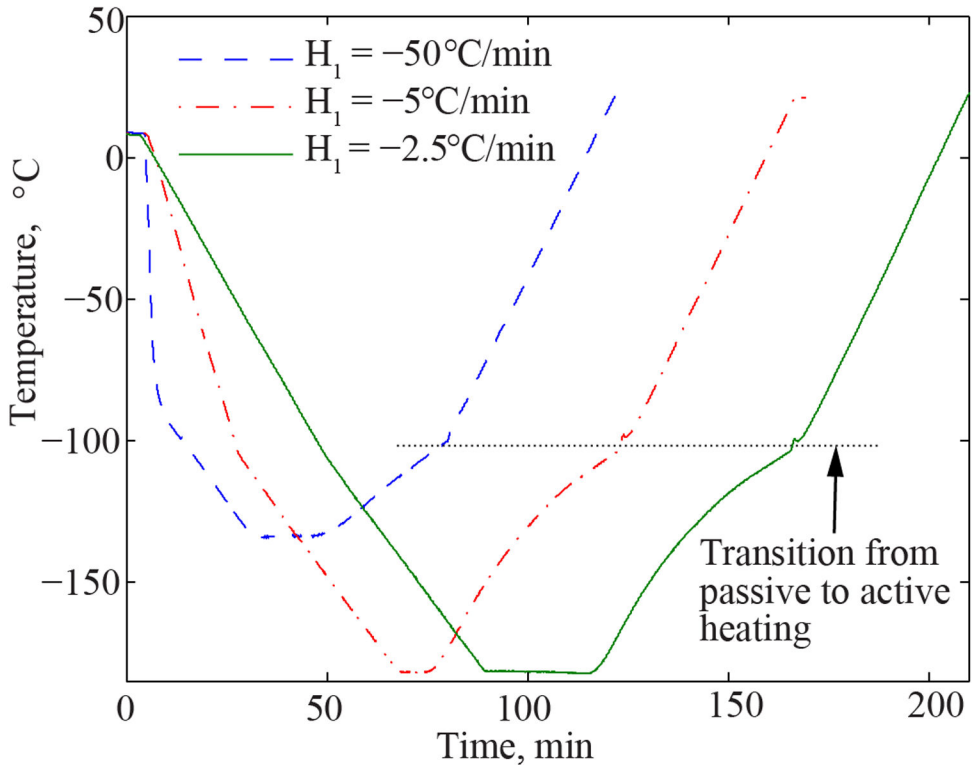

Figure 2.

Representative thermal histories during thermal conductivity measurements of DP6 mixed with PEG400, where temperature data were measured at the center of the cuvette inner wall surface. For all experiments the following rates were kept constant: H_2= −2°C/min, H_3 =1.7°C/min (average passive rewarming), and H_4= 3 °C/min.

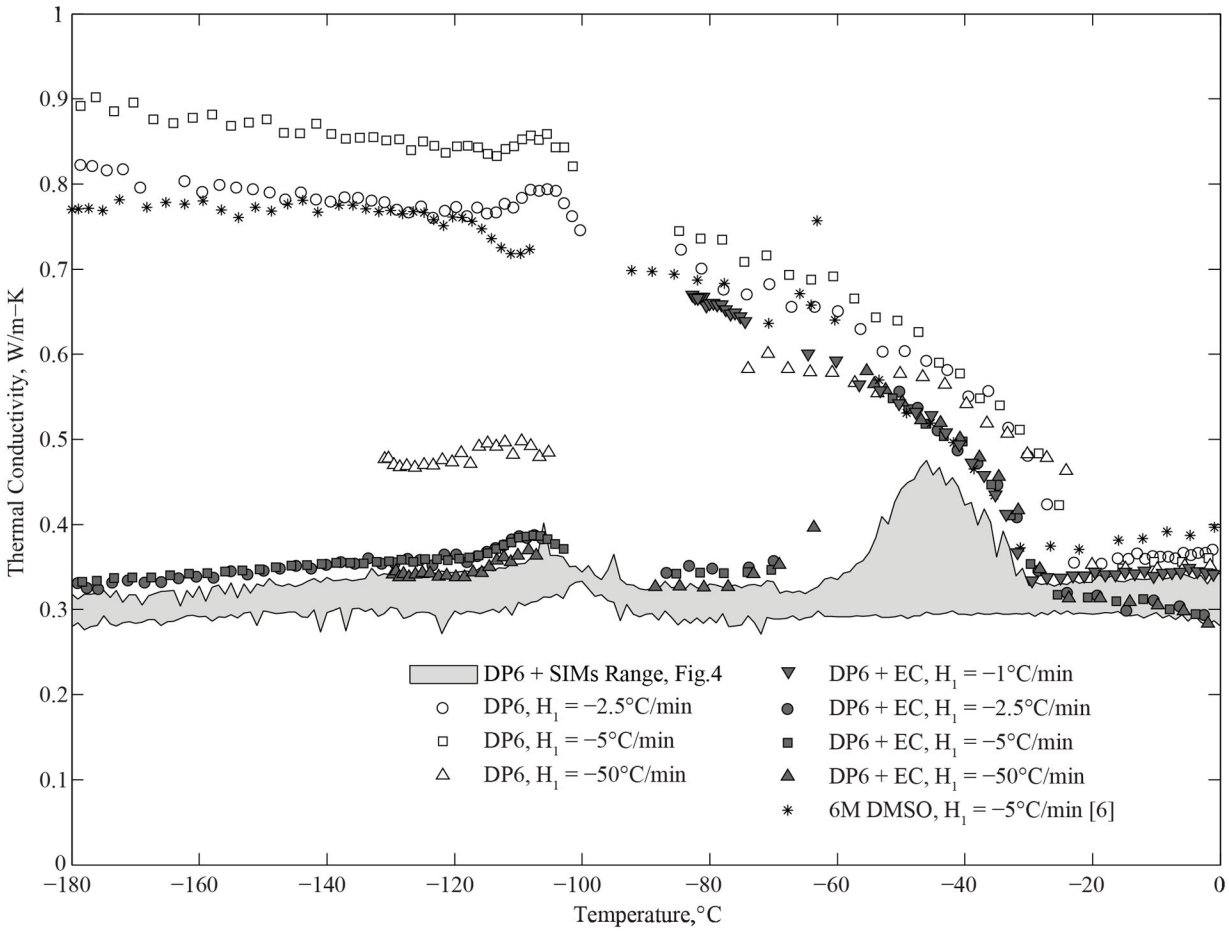

Figure 3.

Measured thermal conductivity of DP6 in the presence and absence of SIMs and EC; 6M DMSO is also shown for reference [6]. At the applicable cooling rate, the glass transition temperature for 6M DMSO is −132 °C, and −119°C for DP6 [13,19]. The eutectic temperature for DMSO is −63°C at a concentration of 6M [20].

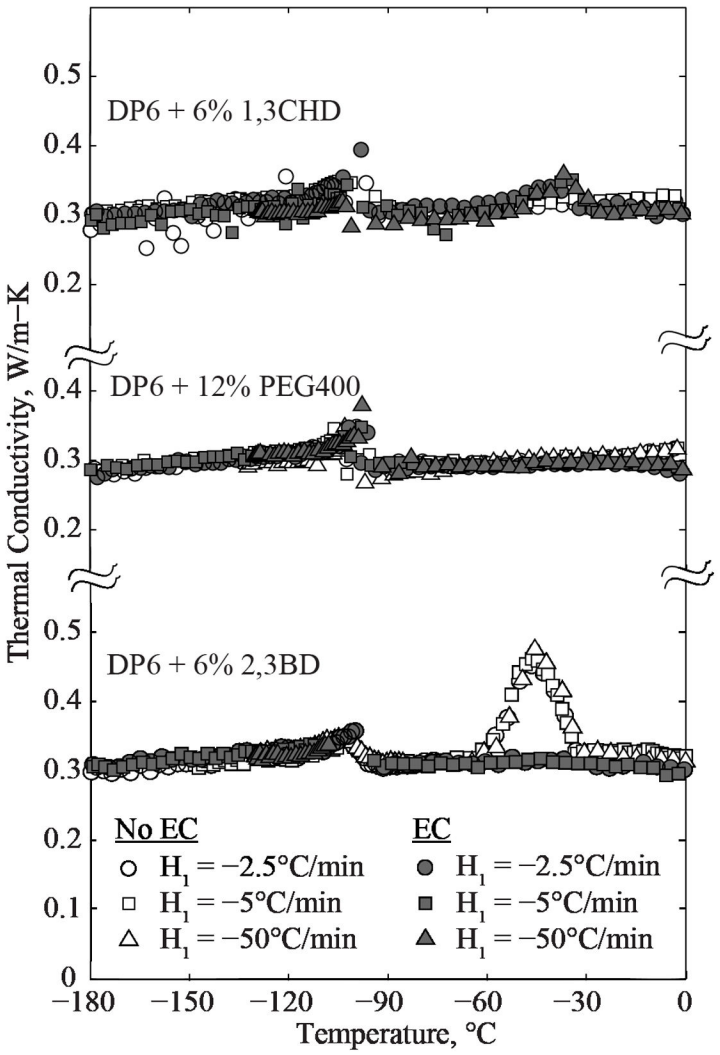

Figure 4.

Thermal conductivity measurements of DP6 in the presence of SIMs, where the glass transition temperature of DP6 is −119°C at the applicable cooling rates [19].

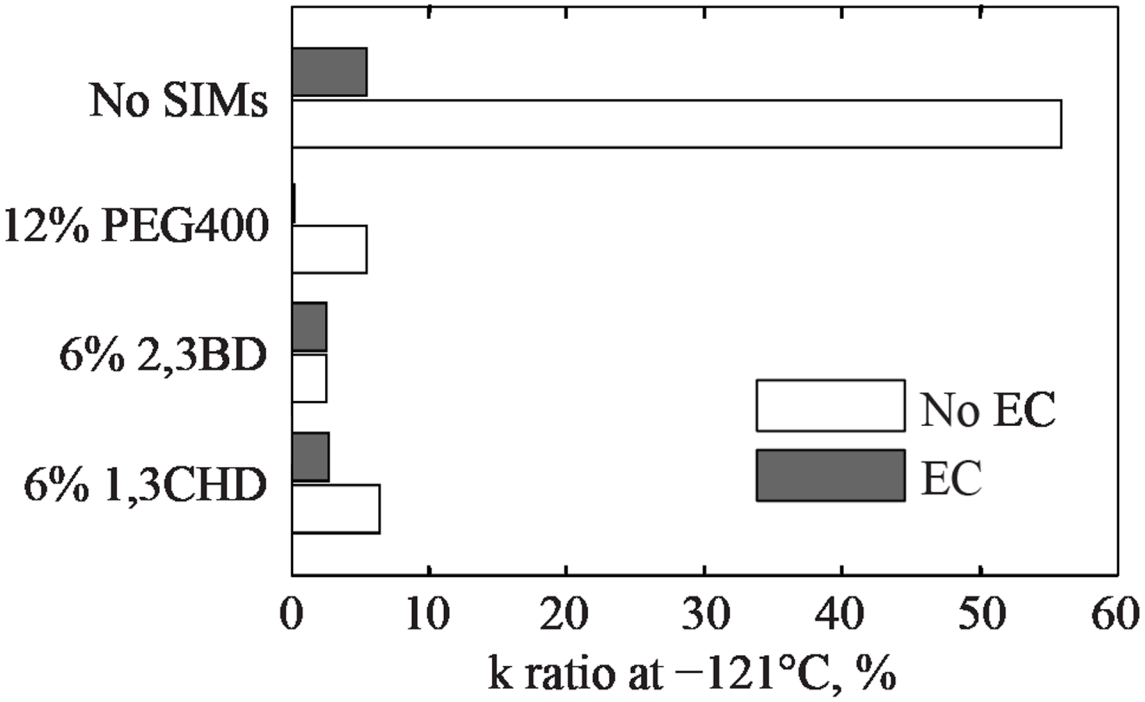

Figure 5.
Average difference in thermal conductivity measurements between a cooling rate of 5°C/min and 50°C/min at −121°C, two degrees below the glass transition temperature of −119°C [19].

Table 1

Summary of thermal history parameters used in this study, where all protocols included H_2= −2°C/min and H_3= 3°C/min as illustrated in Fig. 2.

CPA	Vehicle Solution	H_1, °C/min	T_1, °C	$T_{storage}$, °C
DP6 + 6% 1,3CHD	None	−2.5	−100	−180
		−5	−100	−180
		−50	−80	−130
	Euro-Collins	−2.5	−100	−180
		−5	−100	−180
		−50	−80	−130
DP6 + 6% 2,3BD	None	−2.5	−100	−180
		−5	−100	−180
		−50	−80	−130
	Euro-Collins	−2.5	−100	−180
		−5	−100	−180
		−50	−80	−130
DP6 + 12% PEG400	None	−2.5	−100	−180
		−5	−100	−180
		−50	−80	−130
	Euro-Collins	−2.5	−100	−180
		−5	−100	−180
		−50	−80	−130
DP6	None	−2.5	−100	−180
		−5	−100	−180
		−50	−80	−130
	Euro-Collins	−2.5	−100	−180
		−5	−100	−180
		−50	−80	−130

Table 2

Best-fit polynomial approximation for thermal conductivity curves displayed in Figs 3 and 5, where the temperature is specified in °C and the thermal conductivity is given in; average values are given in cases where (i) the span of the polynomial approximation of thermal conductivity is smaller than two standard deviations of the experimental data over the relevant temperature range (denoted by †), or (ii), where extensive RPC effects over a given data set are observed (denoted by ‡).

CPA-SIM Cocktail	Vehicle Solution	H1, °C/min	Temperature Range, °C	$k=a_0+a_1T+a_2T^2+a_3T^3+a_4T^4+a_5T^5$, W m^{-1}°C^{-1}						R^2
				a_0	a_1	a_2	a_3	a_4	A_5	
DP6 + 6% 1,3CHD	None	−2.5	−180.0 … −112.7	3.85×10^{-1}	4.86×10^{-4}					0.930
			−89.9 … 0.0	3.32×10^{-1}	6.59×10^{-4}	1.10×10^{-5}	1.25×10^{-7}	5.69×10^{-10}		0.919
		−5	−180.0 … −113.2	3.75×10^{-1}	3.97×10^{-4}					0.912
			−85.8 … 0.0	3.30×10^{-1}	5.69×10^{-4}	8.21×10^{-6}	1.09×10^{-7}	6.66×10^{-10}		0.969
		−50	−129.3 … −108.6	3.06×10^{-1}†						-
	EC	−2.5	−180.0 … −116.7	3.74×10^{-1}	4.16×10^{-4}					0.904
			−89.1 … 0.0	3.02×10^{-1}	-8.65×10^{-4}	-2.39×10^{-5}	-3.40×10^{-7}	-1.95×10^{-9}		0.570
		−5	−180.0 … −109.7	3.60×10^{-1}	3.98×10^{-4}					0.912
			−87.0 … 0.0	3.05×10^{-1}‡						-
		−50	−129.0 … −112.1	3.03×10^{-1}†						-
			−79.8 … 0.0	3.02×10^{-1}‡						-
DP6 + 6% 2,3BD	None	−2.5	−180.0 … −119.9	4.00×10^{-1}	4.73×10^{-4}					0.884
			−93.3 … 0.0	3.28×10^{-1}‡						-
		−5	−180.0 … −112.8	3.59×10^{-1}	3.39×10^{-4}					0.723
			−84.2 … 0.0	3.19×10^{-1}‡						-
		−50	−129.7 … −108.8	3.10×10^{-1}†						-
	EC	−2.5	−180.0 … −109.6	3.79×10^{-1}	4.10×10^{-4}					0.903
			−89.6 … 0.0	3.01×10^{-1}	-5.27×10^{-4}	-2.74×10^{-6}	1.11×10^{-7}	1.03×10^{-9}		0.594
		−5	−180.0 … −113.5	3.85×10^{-1}	4.56×10^{-4}					0.906
			−94.3 … 0.0	2.94×10^{-1}	-1.06×10^{-3}	-1.39×10^{-5}	5.05×10^{-8}	1.09×10^{-9}		0.618
		−50	−130.1 … −112.3	3.21×10^{-1}†						-
DP6 + 12% PEG400	None	−2.5	−180.0 … −113.3	3.66×10^{-1}	4.69×10^{-4}					0.928
			−93.6 … 0.0	3.19×10^{-1}	7.53×10^{-4}	4.36×10^{-6}	-6.74×10^{-8}	-6.44×10^{-10}		0.968
		−5	−180.0 … −112.1	3.66×10^{-1}	4.43×10^{-4}					0.940
			−90.7 … 0.0	3.18×10^{-1}	7.84×10^{-4}	1.15×10^{-5}	8.67×10^{-8}	3.11×10^{-10}		0.961
		−50	−131.7 … −112.6	2.96×10^{-1}†						-
			−90.7 … 0.0	3.21×10^{-1}	9.54×10^{-4}	3.58×10^{-6}	-8.59×10^{-7}	-2.01×10^{-8}	-1.21×10^{-10}	0.985

CPA-SIM Cocktail	Vehicle Solution	H1, °C/min	Temperature Range, °C	$k=a0+a1T+a2T^2+a3T^3+a4T^4+a5T^5$, W m^{-1}·$°C^{-1}$						R^2
				a0	*a1*	*a2*	*a3*	*a4*	*A5*	
DP6	EC	−2.5	−180.0 … −109.8	3.59×10^{-1}	4.17×10^{-4}					0.919
			−93.7 … 0.0	2.82×10^{-1}	-1.08×10^{-3}	-2.67×10^{-5}	-2.23×10^{-7}	-5.16×10^{-10}		0.970
		−5	−180.0 … −110.7	3.63×10^{-1}	4.25×10^{-4}					0.913
			−91.1 … 0.0	2.91×10^{-1}	-5.10×10^{-4}	-1.19×10^{-5}	-3.94×10^{-8}	4.08×10^{-10}		0.803
		−50	−129.5 … −108.7	3.11×10^{-1}†						-
			−84.7 … 0.0	2.90×10^{-1}	-4.65×10^{-4}	-4.32×10^{-6}	1.77×10^{-7}	2.12×10^{-9}	-4.10×10^{-14}	0.839
	None	−2.5	−180.0 … −40.7	4.29×10^{-1}	-2.91×10^{-3}	3.11×10^{-5}	4.10×10^{-7}	1.20×10^{-9}		0.990
			−40.7 … −22.9	-2.65×10^{-1}	-3.52×10^{-2}	-3.58×10^{-4}				0.983
			−22.9… 0.0	3.70×10^{-1}	7.03×10^{-4}					0.887
		−5	−180.0 … −35.5	3.01×10^{-1}	-8.06×10^{-3}	-2.96×10^{-5}	4.45×10^{-8}	3.52×10^{-10}		0.994
			−35.5 … −20.9	-2.79×10^{-1}	-3.90×10^{-2}	-4.41×10^{-4}				0.988
			−20.9 … 0.0	3.61×10^{-1}	9.07×10^{-4}					0.898
		−50	−131.2 … −117.5	4.72×10^{-1}†						-
	EC	−1	−82.8 … −29.8	-1.81×10^{0}	-1.46×10^{-1}	-3.46×10^{-3}	-3.68×10^{-5}	-1.44×10^{-7}		0.998
			−29.8 … 0.0	3.43×10^{-1}	-1.47×10^{-4}	-1.23×10^{-5}				0.483
		−2.5	−180.0 … −118.9	4.32×10^{-1}	5.85×10^{-4}					0.909
			−86.7 … −67.8	4.07×10^{-1}	7.29×10^{-4}					0.714
			−50.2 … −27.6	-6.06×10^{0}	-5.99×10^{-1}	-2.08×10^{-2}	-3.23×10^{-4}	-1.86×10^{-6}		0.998
			−27.6 … 0.0	2.95×10^{-1}	-1.20×10^{-3}	-6.17×10^{-6}				0.763
		−5	−180.0 … −117.7	4.19×10^{-1}	4.74×10^{-4}					0.979
			−85.3 … −70.3	3.44×10^{-1}†						-
			−52.3 … −26.6	1.57	1.94×10^{-1}	9.50×10^{-3}	1.83×10^{-4}	1.24×10^{-6}		0.989
			−26.6 … 0.0	2.83×10^{-1}	-2.97×10^{-3}	-7.22×10^{-5}				0.970
		−50	−129.8 … −117.1	3.42×10^{-1}†						-
			−88.6 … −75.2	3.28×10^{-1}†						-
			−54.2 … −27.3	−1.72	-1.51×10^{-1}	-3.73×10^{-3}	-3.92×10^{-5}	-1.33×10^{-7}		0.996
			−26.7 … 0.0	2.81×10^{-1}	-3.06×10^{-3}	-6.77×10^{-5}				0.986